



## SECONDARY NEUTRON AND PROTON PRODUCTION IN PROTON-INDUCED REACTIONS WITH $^{12}\text{C}$ , $^{14}\text{N}$ AND $^{16}\text{O}$ NUCLEI

 Rustam Murtazin<sup>1\*</sup>,  Stepan Karpus<sup>2,1</sup>

<sup>1</sup>National Science Center "Kharkiv Institute of Physics and Technology", 1 Akademichna, Kharkiv, 61108, Ukraine

<sup>2</sup>Lutsk National Technical University, 75, Lvivska, Lutsk, 43018, Ukraine

\*Corresponding Author e-mail: [rumurtazin@gmail.com](mailto:rumurtazin@gmail.com)

Received July 24, 2025; revised October 3, 2025; in final form October 29, 2025; accepted November 3, 2025

The results of computer simulation of the secondary neutrons and protons yield per one incident proton during the interaction of protons with an energy of 50 MeV with light nuclei -  $^{12}\text{C}$ ,  $^{14}\text{N}$  and  $^{16}\text{O}$  using the TALYS - 1.96 code by default are presented. The importance of taking into account the radiation of secondary nucleons - neutrons and protons is a necessary element in conducting fundamental and applied nuclear research, such as dosimetry and radiation safety. As a result, the values of the total cross section for the secondary neutrons and protons production were obtained, that indicate significant differences in their energy range dependencies versus the target nucleus. For the nucleus  $^{12}\text{C}$ , the threshold for the production of neutrons is in the region of 20 MeV. A similar characteristic for  $^{14}\text{N}$  lies in the region of up to 10 MeV, and for  $^{16}\text{O}$  the total neutron production threshold is 17-18 MeV. The maximum neutron yield per incident proton is observed for the  $^{16}\text{O}$  nucleus. The total secondary proton production cross-section and their yield were also determined. In the case of proton yield, the oxygen nucleus demonstrates the largest number of secondary protons per proton, which is 1.47. The calculated values of the energy differential cross-section of the secondary radiation of protons and neutrons were also obtained. The maximum average energy of secondary protons is observed for the  $^{14}\text{N}$  nucleus and is 12.72 MeV, while for the  $^{12}\text{C}$  and  $^{16}\text{O}$  nuclei it is about 10 MeV. Analysis of the energy differential cross-section of secondary neutrons showed that the maximum average energy is possessed by neutrons formed as a result of interaction with the nitrogen nucleus, while the energies of secondary neutrons formed on the nuclei of  $^{12}\text{C}$  and  $^{16}\text{O}$  are approximately equal (6.2 and 6.4, respectively).

**Keywords:** Light nuclei; Secondary nucleons, TALYS

**PACS:** 25.40-h, 87.53.Bn

### 1. INTRODUCTION

Interactions of medium-energy protons (tens to hundreds of MeV) with materials containing light elements such as Carbon - 12, Nitrogen - 14, and Oxygen - 16 are of significant scientific and practical interest. These elements are fundamental constituents of biological objects, air, various shielding materials, and components of detectors used in radiation fields. Proton beams in this energy range are extensively utilized in fundamental nuclear research and notably in proton therapy for cancer treatment. Beyond these applied aspects, a thorough understanding of proton-nucleus interactions at intermediate energies, including the precise characterization of all emitted particles, is crucial for fundamental nuclear physics. Such data provide stringent tests for nuclear reaction models, help refine our knowledge of nuclear structure, nucleon-nucleon interactions within the nuclear medium, and mechanisms of particle production like pre-equilibrium emission and compound nucleus decay. Accurate cross-section and spectral data for proton-induced reactions on light nuclei are also essential for benchmarking and improving nuclear data libraries used in various simulation codes.

Accurate assessment of the radiation field characteristics and its subsequent effects, including absorbed dose and radiation damage, is determining for all these applications. While the primary proton beam is the initial source of radiation, its interaction with the nuclei of the traversed medium leads to the generation of a complex secondary radiation field. This field comprises not only scattered primary protons but also a variety of secondary particles, such as neutrons, light charged particles (protons, deuterons, alpha particles), and heavier residual nuclei.

These secondary particles often possess a broad spectrum of energies and wide angular distributions. They can contribute significantly to the total energy deposition, linear energy transfer (LET) distributions, and thus to the relative biological effectiveness (RBE) of the radiation, sometimes in regions considerably distant from the primary beam path or even outside the target volume. Consequently, neglecting or inadequately accounting for the contribution of these secondary particles can lead to substantial inaccuracies in dosimetry calculations, treatment planning in proton therapy (e.g., out-of-field doses), or underestimation of radiation-induced damage in materials and electronic components.

An issue of secondary emission for many years is important point that holds the attention of scientific literature and this aspect of experimental nuclear physics is still considered as critical question, the number of studies were carried out to research the emission properties and effects of secondary interaction [1, 2, 3]. Moreover, in experimental nuclear physics employing track detectors such as streamer chambers or bubble chambers for studying proton-induced reactions, the presence of secondary particles generated within target or detector volume can significantly complicate an analysis. These secondaries can imitate or distort the signatures of the primary reaction products, leading to potential misidentification

of event topologies (e.g., two-, three-, four-, or five-pointed events) and systematic errors in the determination of reaction cross-sections and particle kinematics.

The primary objective of this work is to computationally investigate and highlight the importance of secondary protons and neutrons produced during the interaction of 50 MeV protons with  $^{12}\text{C}$ ,  $^{14}\text{N}$ , and  $^{16}\text{O}$  nuclei. Utilizing the nuclear reaction code TALYS - 1.96, the energy spectra, total production cross-sections, and yields of these secondary nucleons were calculated. The results aim to demonstrate the significant contribution of these secondary particles to the overall radiation environment and to underscore the necessity of their explicit consideration for comprehensive and accurate radiation exposure assessments in contexts involving carbon-, nitrogen-, and oxygen-containing materials.

## 2. METHODS OF CALCULATION

The nuclear reaction calculations for the interaction of protons with  $^{12}\text{C}$ ,  $^{14}\text{N}$ , and  $^{16}\text{O}$  target nuclei were performed using the TALYS code, version 1.96 [4]. TALYS is a versatile nuclear reaction code capable of simulating the basic types of nuclear reactions in the energy range up to several hundred megaelectronvolts.

For all calculations, the default physical models and parameters embedded in TALYS - 1.96 were utilized. Based on the TALYS output files (and a list of input parameters previously provided by user), the key default settings include:

**Nuclear Masses:** Experimental nuclear mass values from current databases were used. In cases where experimental data were unavailable for certain intermediate or daughter nuclei, TALYS employed theoretical masses calculated using the Duflo-Zuker model[5].

**Optical Model Potential (OMP):** A local optical potential model was used for the interaction of nucleons (protons and neutrons) with nuclei. This implies that TALYS attempts to select the best OMP parameters from its local library for the specific nuclide and energy, what is often based on the global phenomenological Koning-Delaroche potential [6] for nucleons. For alpha particles, the Avrigeanu parameterization was used, and for deuterons, a standard phenomenological parameterization was retained.

**Nuclear Level Densities (LD):** A complex model was used, putting together the Constant Temperature Model (CTM) at low excitation energies with the Fermi Gas Model (FGM) at higher energies [7]. Shell corrections were accounted for using the Myers-Swiatecki model[8].

**Pre-equilibrium Processes:** The contribution from pre-equilibrium decay was calculated based on the two-component exciton model, that distinguishes between proton and neutron degrees of freedom, utilizing Williams formula [9] for the particle-hole state density.

**Statistical Decay (Compound Nucleus):** The decay of the compound nucleus is described within the framework of the Hauser-Feshbach statistical model, including width fluctuation corrections according to the Moldauer model [10, 11].

**Gamma-ray Emission:** For E1 transitions, the Kopecky-Uhl generalized Lorentzian (GLO) model [12] was used, and for M1 transitions, a standard Lorentzian (SMLO) [13] model was employed.

**Fission:** Fission channel calculations were disabled, as expected for light target nuclei.

The calculations were performed for incident proton energies ranging from 5 MeV to 50 MeV with a 1 MeV step. The yields of primary nucleons that was analyzed demonstrate the effects of secondary particles of the secondary nucleons energy differential cross-section at incident proton energy of 50 MeV, as well as the total production cross-sections and yields of these particles as a function of incident proton energy.

## 3. RESULTS

This section presents the results obtained from TALYS - 1.96 simulations for the interaction of protons with  $^{12}\text{C}$ ,  $^{14}\text{N}$ , and  $^{16}\text{O}$  nuclei, focusing on the production of secondary protons and neutrons.

### 3.1. Total Production Cross-Sections and Secondary Neutron and Proton Yields

The calculated total neutron production cross-sections as a function of incident proton energy ( $E_p$ ) for  $^{12}\text{C}$ ,  $^{14}\text{N}$ , and  $^{16}\text{O}$  targets are presented in Figure 1a.

For the  $^{12}\text{C}$  target, neutron production indicates a threshold energy around 20 MeV, that corresponds to the Q-value of the most likely neutron-producing channel, e.g.,  $^{12}\text{C}(p, n)^{12}\text{N}$  ( $Q \approx -18.1$  MeV). Above this threshold, the cross-section rises steadily with increasing incident proton energy, reaching approximately 156.1 mb at 50 MeV. The corresponding neutron yield (average number of neutrons produced per incident proton) at 50 MeV is 0.4.

The  $^{14}\text{N}$  target shows an earlier seizure of neutron production, with a reasonable threshold below 10 MeV, consistent with the Q-value for the  $^{14}\text{N}(p, n)^{14}\text{O}$  reaction ( $Q \approx -5.9$  MeV). The cross-section enlarges with energy, though with a less steep slope compared to  $^{12}\text{C}$  in some energy regions, and reaches about 199.8 mb at 50 MeV. The neutron yield at 50 MeV for  $^{14}\text{N}$  is 0.46.

For the  $^{16}\text{O}$  target, the threshold for neutron production is marked around 17-18 MeV, which aligns with the Q-value for the  $^{16}\text{O}(p, n)^{16}\text{F}$  reaction ( $Q \approx -16.2$  MeV). Similar to  $^{12}\text{C}$ , the cross-section increases with incident energy, attaining a value of approximately 214.1 mb at 50 MeV. The neutron yield at this energy is 0.46.

Comparing the three targets at 50 MeV, the total neutron production cross-section is highest for  $^{16}\text{O}$ , followed by  $^{14}\text{N}$ , and then  $^{12}\text{C}$ . The neutron yields at 50 MeV are comparable for  $^{14}\text{N}$  and  $^{16}\text{O}$ , and somewhat lower for  $^{12}\text{C}$ .

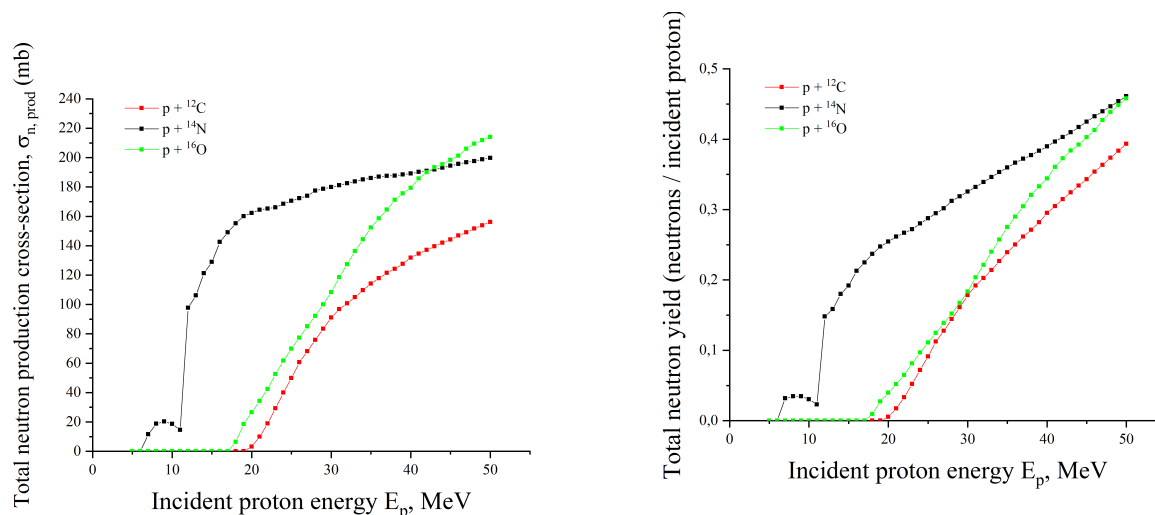


**Figure 1.** The dependence of total neutron production cross-section (a) and total neutron yield (b) versus incident proton energy  $E_p$

### 3.1.1. Proton production

The total proton production cross-sections, which include contributions from elastically scattered primary protons as well as secondary emitted protons, are shown as a function of incident proton energy ( $E_p$ ) in Figure 2.

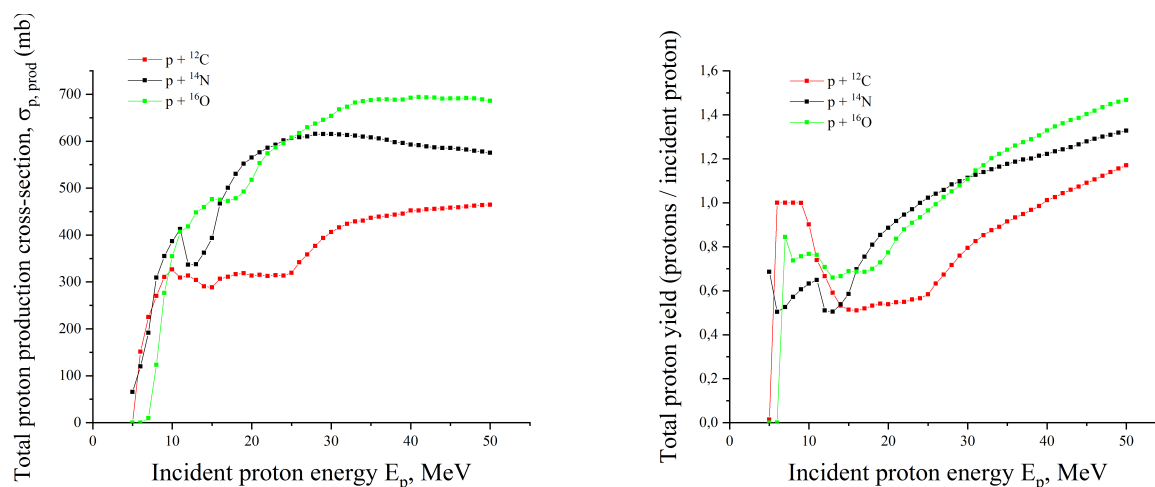


**Figure 2.** The dependence of total proton production cross-section (a) and total proton yield (b) versus incident proton energy  $E_p$

For all three targets:  $^{12}\text{C}$ ,  $^{14}\text{N}$ , and  $^{16}\text{O}$  - the total proton production cross-section is non-zero even at the lowest incident energies considered (5-7 MeV), primarily due to elastic scattering. As the incident energy increases, the cross-sections generally rise. For  $^{12}\text{C}$ , the cross-section rises from a small value, increases significantly up to around 25-30 MeV, and then shows a more gradual raise, reaching approximately 464.3 mb at 50 MeV. The corresponding total proton yield at 50 MeV is 1.17, indicating that, on average, more than one proton exits the interaction per incident proton, confirming the production of secondary protons in addition to the scattered primary ones.

The  $^{14}\text{N}$  target exhibits a considerable proton production cross-section across the energy range, starting around 65.6 mb at 5 MeV and expanding to about 575.3 mb at 50 MeV. The yield for  $^{14}\text{N}$  at 50 MeV is 1.33.

For  $^{16}\text{O}$ , a notable proton production cross-section begins around 7 MeV. It increases with energy, reaching approximately 686.1 mb at 50 MeV, the highest among the three targets. The total proton yield for  $^{16}\text{O}$  at 50 MeV is 1.47.

A comparison at 50 MeV shows that  $^{16}\text{O}$  has the largest total proton production cross-section and yield, followed by  $^{14}\text{N}$ , and then  $^{12}\text{C}$ . The yields consistently greater than one for all targets at higher energies (above  $\sim 26$  MeV for  $^{16}\text{O}$ ,  $\sim 25$  MeV for  $^{14}\text{N}$ , and  $\sim 40$  MeV for  $^{12}\text{C}$ , based on the provided data) plainly demonstrate the significant role of secondary proton emission alongside the primary scattered protons.

### 3.2. Energy differential cross-sections of secondary nucleons at 50 MeV incident proton energy

#### 3.2.1. Proton energy differential cross-sections

The energy differential cross-sections of protons formed in the interaction of 50 MeV incident protons with  $^{12}\text{C}$ ,  $^{14}\text{N}$ , and  $^{16}\text{O}$  targets are presented in Figure 3.

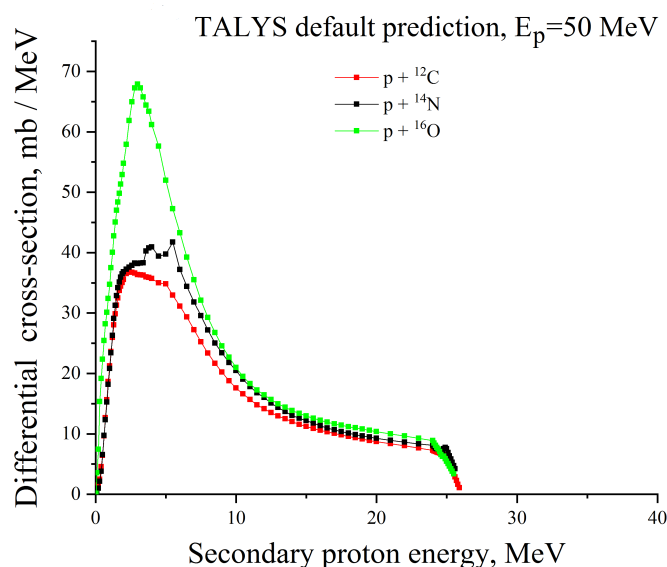


**Figure 3.** The differential cross-section versus secondary proton energy  $E_p$

For all three nuclei, the energy differential cross-sections exhibit identical features. A plateau is observed at the highest outgoing proton energies, approaching the incident energy of 50 MeV. This peak primarily corresponds to elastically and quasi-elastically scattered primary protons. Below 25 MeV, a broad area extends towards lower energies, representing the contribution of secondary protons produced through various inelastic processes (such as direct knock-out or pre-equilibrium emission), as well as primary protons that have undergone significant energy loss.

The intensity and shape of this continuous part of the energy differential cross-section vary for the different targets. For  $^{12}\text{C}$ , the continuous energy differential cross-section of secondary protons contributes significantly, with an average outgoing proton energy (including the elastic peak) of 10.21 MeV. For  $^{14}\text{N}$ , the secondary proton component also appears substantial, and the average energy of all outgoing protons is 12.72 MeV. In the case of  $^{16}\text{O}$ , the average outgoing proton energy is 10.67 MeV.

The presence of a significant number of protons at energies much lower than incident energy, as shown by the continuous part of the energy differential cross-sections and the relatively low average outgoing proton energies, points out the importance of secondary proton production. These lower-energy secondary protons can have different transport properties and biological effectiveness compared to the primary 50 MeV protons.

#### 3.2.2. Neutron energy differential cross-sections

The energy differential cross-sections of neutrons produced from the interaction with incident protons with  $^{12}\text{C}$ ,  $^{14}\text{N}$ , and  $^{16}\text{O}$  targets are depicted in Figure 4.

Unlike the proton energy differential cross-sections, the neutron energy differential cross-sections do not exhibit a prominent peak corresponding to elastically scattered incident particles. Instead, they are characterized by continuous

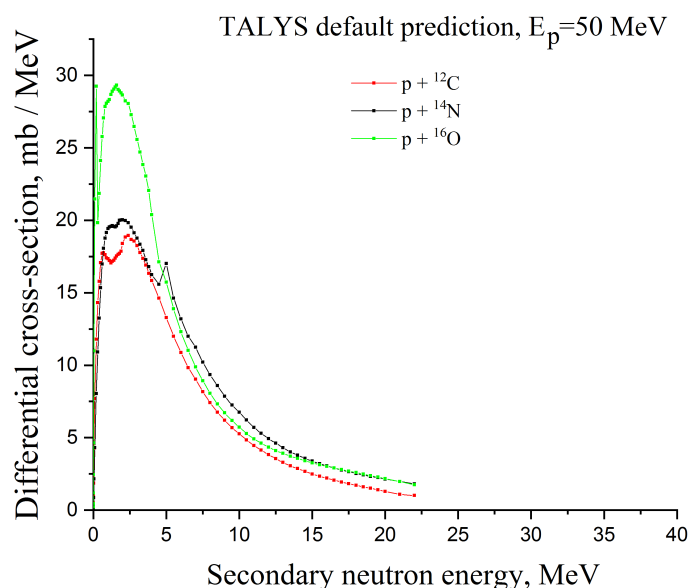


**Figure 4.** The differential cross-section versus secondary neutron energy  $E_n$

distributions, primarily reflecting neutrons emitted through compound nucleus stage and pre-equilibrium processes. These processes typically result in a wide distribution of neutron energies, extending from very low energies up to a significant fraction of the available energy.

For the  $^{12}\text{C}$  target, the neutron energy differential cross-section shaped by the majority of neutrons emitted at lower energies. The average energy of outgoing neutrons is 6.2 MeV.

The neutron energy differential cross-section for the  $^{14}\text{N}$  target also displays a extended distribution, with an average outgoing neutron energy of 8.95 MeV. This higher average energy compared to  $^{12}\text{C}$  suggests a relatively harder neutron energy differential cross-section from  $^{14}\text{N}$  under these conditions.

In the case of  $^{16}\text{O}$ , the neutron energy differential cross-section has continuous outline, with an average outgoing neutron energy of 6.36 MeV, which is comparable to that from  $^{12}\text{C}$ .

The shapes of these energy differential cross-sections indicate that a large number of neutrons are produced with a wide range of energies. These secondary neutrons, particularly those with higher energies, can travel significant distances in materials and contribute to a dose deposition and radiation effects far from the initial interaction site, highlighting their importance in radiation shielding and dosimetry assessments. The differences in shapes of energy differential cross-section and average energies among the targets reflect the underlying nuclear structure and reaction dynamics specific to each nuclide.

To provide a quantitative summary of the secondary nucleon production from the interaction of 50 MeV protons with  $^{12}\text{C}$ ,  $^{14}\text{N}$ , and  $^{16}\text{O}$ , main integral characteristics are compiled in Table 1.

**Table 1.** Summary of calculated integral characteristics for secondary nucleon production from 50 MeV proton interactions with  $^{12}\text{C}$ ,  $^{14}\text{N}$ , and  $^{16}\text{O}$

Characteristic	$^{12}\text{C}$	$^{14}\text{N}$	$^{16}\text{O}$
Total neutron production cross-section, mb	156.15	199.8	214.1
Neutron yield (neutrons/incident proton), n	0.4	0.46	0.46
Average outgoing neutron energy, MeV	6.2	8.95	6.36
Total proton production cross-section†, mb	464.32	575.32	686.1
Proton yield (protons/incident proton)†, n	1.17	1.33	1.47
Average outgoing proton energy, MeV	10.21	12.71	10.67

† Includes contributions from elastically/quasi-elastically scattered primary protons.

This table includes the total production cross-sections for neutrons and protons, their respective yields (average number of particles produced per incident proton), and the average energies of the emitted secondary protons and neutrons at an incident proton energy of 50 MeV.

These tabulated values, along with the presented energy differential cross-sections and production cross-section excitation functions, provide a comprehensive overview of secondary proton and neutron generation for the studied targets. The data clearly indicate substantial production of secondary nucleons, with distinct characteristics depending on the target nucleus. A detailed interpretation of these findings and their implications will be discussed in the following section.

## 4. DISCUSSION

The results obtained from TALYS - 1.96 simulations provide valuable insights into the production of secondary protons and neutrons when 50 MeV protons interact with  $^{12}\text{C}$ ,  $^{14}\text{N}$ , and  $^{16}\text{O}$  nuclei. This section discusses the interpretation of these findings, particularly concerning their significance for radiation exposure assessments.

### 4.1. Interpretation of key findings and significance of secondary nucleons

The key findings presented in Section 3 highlight that the interaction of 50 MeV protons with carbon, nitrogen, and oxygen leads to a serious generation of secondary nucleons. Specifically, the total neutron production yields at 50 MeV were found to be 0.4 for  $^{12}\text{C}$ , 0.46 for  $^{14}\text{N}$ , and 0.46 for  $^{16}\text{O}$ , indicating that nearly half a neutron is produced on average per incident proton for nitrogen and oxygen targets. Similarly, total proton yields (which include scattered primary protons and produced secondary protons) were 1.17 for  $^{12}\text{C}$ , 1.33 for  $^{14}\text{N}$ , and 1.47 for  $^{16}\text{O}$ . Yields greater than unity for proton production directly confirm the creation of secondary protons.

The energy differential cross-sections of these secondary nucleons, that are presented in Fig. 2 and Fig. 3, further underscore their importance. The proton energy differential cross-sections in the Fig. 2 are characterized by a significant range of lower-energy protons in addition to the elastic/quasi-elastic peak. The average energies of all outgoing protons (10.21 MeV for  $^{12}\text{C}$ , 12.72 MeV for  $^{14}\text{N}$ , and 10.67 MeV for  $^{16}\text{O}$ ) are considerably lower than the 50 MeV incident energy, indicating that a large fraction of the energy is transferred to generating these secondary protons or lost in inelastic interactions. These lower-energy protons can possess higher Linear Energy Transfer (LET) values and, consequently, an increased Relative Biological Effectiveness (RBE), which is a critical factor in radiotherapy and radiation protection.

The neutron energy differential cross-sections in the Fig. 3 are continuous, with average outgoing neutron energies of 6.2 MeV for  $^{12}\text{C}$ , 8.945 MeV for  $^{14}\text{N}$ , and 6.362 MeV for  $^{16}\text{O}$ . These neutrons, being uncharged, can penetrate deeper into materials and tissues, contributing to the dose deposition in regions distant from the primary proton beam path, including sensitive organs or electronic components outside the intended target volume. The production of such a significant flux of secondary neutrons with a broad energy distribution necessitates their careful consideration in shielding design and for accurate out-of-field dose estimations in proton therapy.

Neglecting these secondary protons and neutrons would lead to a serious underestimation of the total absorbed dose, an incorrect assessment of the radiation quality (average LET and RBE), and potentially compromised outcomes in applications such as radiotherapy planning or radiation risk assessment for personnel and equipment. Therefore, the explicit inclusion of secondary nucleon production data, such as those generated in this study, is crucial for accurate modeling of radiation transport and its effects in C, N, and O-containing media.

Furthermore, from a fundamental physics perspective, the detailed energy differential cross-sections and production cross-sections of secondary nucleons serve as valuable experimental observables (even if computationally derived or based on established models) for testing and constraining theoretical models of nuclear reactions. Discrepancies or agreements between TALYS predictions and potential future experimental data for these systems can provide understanding of employed models for optical potentials, level densities, and pre-equilibrium decay mechanisms, particularly for light nuclei where such comprehensive data might be sparse.

The production of such a significant flux of secondary neutrons with a broad energy distribution requires their careful consideration in shielding design and for accurate out-of-field dose estimations in proton therapy. Beyond dosimetric and radiation protection aspects, the substantial yields and specific energy distributions of secondary protons and neutrons, as calculated in this work, have direct implications for the interpretation of experimental data obtained from proton-nucleus interaction studies, particularly those utilizing visual track detectors like streamer chambers. For instance, secondary protons originating from primary interactions within the target or the gas inside a chamber can create additional tracks that may be erroneously attributed to the primary reaction vertex. This can lead to a misinterpretation of the multiplicity of charged particles in an event, potentially distorting the analysis of few-pointed (e.g., two-, three-, four-, or five-pointed) event topologies which are often crucial for identifying specific reaction channels. The continuous energy differential cross-sections of these secondaries, especially the lower-energy component, mean they will have varying ranges and ionization densities, further complicating track reconstruction and particle identification.

Similarly, while secondary neutrons are not directly visible in such chambers, their subsequent interactions within the detector volume or surrounding materials can produce tertiary charged particles (e.g., recoil protons), creating spurious tracks or increasing the overall background. The calculated neutron yields (approaching 0.5 neutrons per incident proton for  $^{14}\text{N}$  and  $^{16}\text{O}$  at 50 MeV) indicate a non-negligible probability of such effects. Therefore, proper simulation of secondary particle production, as provided by codes like TALYS, is essential not only for theoretical understanding but also as a crucial input for Monte Carlo simulations used to correct experimental data for such distortions and to properly estimate detector acceptance and efficiency. This underscores the necessity for both experimentalists and theoreticians to account for the entire energy differential cross-section of secondary particles when analyzing proton-nucleus collisions.

## 4.2. Comparative analysis of secondary particle production from $^{12}\text{C}$ , $^{14}\text{N}$ , and $^{16}\text{O}$

The results presented indicate distinct differences in the production characteristics of secondary neutrons and protons for  $^{12}\text{C}$ ,  $^{14}\text{N}$ , and  $^{16}\text{O}$  targets when bombarded with 50 MeV protons, as summarized in Table 1.

Regarding neutron production, the total neutron production cross-section at 50 MeV increases with target mass, being approximately 156.1 mb for  $^{12}\text{C}$ , 199.8 mb for  $^{14}\text{N}$ , and 214.1 mb for  $^{16}\text{O}$ . A similar trend is observed for neutron yields, which are 0.4, 0.46, and 0.46 for  $^{12}\text{C}$ ,  $^{14}\text{N}$ , and  $^{16}\text{O}$ , respectively. This suggests that heavier nuclei in this light-mass range offer more nucleons for interaction, leading to a higher probability of neutron emission. Interestingly, the average energy of outgoing neutrons is notably higher for  $^{14}\text{N}$  (8.95 MeV) compared to  $^{12}\text{C}$  (6.2 MeV) and  $^{16}\text{O}$  (6.4 MeV). This could be attributed to differences in the Q-values of dominant neutron-producing reaction channels (e.g., (p,n)), neutron separation energies, and the level density distributions of the respective residual nuclei. For instance,  $^{14}\text{N}$  is an odd-odd nucleus, which might influence its reaction pathways and energy distributions of emitted particles compared to the even-even  $^{12}\text{C}$  and  $^{16}\text{O}$  nuclei.

For proton production (including scattered primary protons and emitted secondary protons), a similar tendency of increasing total production cross-section and yield with target mass is observed at 50 MeV. The cross-sections are 464.3 mb for  $^{12}\text{C}$ , 575.3 mb for  $^{14}\text{N}$ , and 686.1 mb for  $^{16}\text{O}$ , with corresponding yields of 1.17, 1.33, and 1.47. The average energy of all outgoing protons is also highest for  $^{14}\text{N}$  (12.72 MeV), followed by  $^{16}\text{O}$  (10.67 MeV), and then  $^{12}\text{C}$  (10.21 MeV). The higher average proton energy for  $^{14}\text{N}$  might reflect differences in the balance between elastic/quasi-elastic scattering and the emission of lower-energy secondary protons. The Coulomb barrier will influence the emission of low-energy charged particles, but for outgoing proton energies observed, various reaction mechanisms like (p, p'), (p, 2p), and (p, pn) contribute, and their relative importance can vary with the target nucleus structure.

These target-specific differences in both neutron and proton production highlight the importance of using nuclide-specific data in applications requiring precise radiation transport calculations and dose estimations. The observed variations likely stem from a combination of factors, including nuclear size, binding energies of nucleons, individual Q-values for various open reaction channels, and the specific nuclear structure (e.g., shell effects) influencing level densities and decay paths.

## Acknowledgments

The authors of the article express their sincere gratitude to the Defense Forces of Ukraine for their courage, dedication, and defense of the country. Glory to Ukraine!

## ORCID

 **Rustam Murtazin**, <https://orcid.org/0009-0003-5197-8252>;  **Stepan Karpus**, <https://orcid.org/0000-0002-1087-9245>

## REFERENCES

- [1] T. Oyama, T. Sanami, H. Yashima, *et al.*, Nuclear Instruments and Methods in Physics Research Section A: Accelerators, Spectrometers, Detectors and Associated Equipment, **990**, 164977 (2021). <https://doi.org/10.1016/j.nima.2020.164977>
- [2] A. Shor, and R. Longacre, Physics Letters B, **218**, 100, (1989). [https://doi.org/10.1016/0370-2693\(89\)90483-8](https://doi.org/10.1016/0370-2693(89)90483-8)
- [3] V.I. Gol'danskii, A.E. Ignatenko, *et al.*, Phys. Rev. **109**, 1762 (1958). <https://doi.org/10.1103/PhysRev.109.1762>
- [4] <https://nds.iaea.org/talys/>
- [5] J. Duflo, and A. Zuker, Physical Review C, **52**(1), R23 (1995). <https://doi.org/10.1103/PhysRevC.52.R23>
- [6] A. Koning, and J. Delaroche, Nuclear Physics A, **713**(3-4), 231 (2003). [https://doi.org/10.1016/S0375-9474\(02\)01321-0](https://doi.org/10.1016/S0375-9474(02)01321-0)
- [7] A. Gilbert, and A. Cameron, Canadian Journal of Physics, **43**(8), 1446 (1965). <https://doi.org/10.1139/p65-139>
- [8] W.D. Myers, and W.J. Swiatecki, Nucl. Phys. **81**, 1 (1966). [https://doi.org/10.1016/S0029-5582\(66\)80001-9](https://doi.org/10.1016/S0029-5582(66)80001-9)
- [9] F.C. Williams, Nucl. Phys. A, **166**, 231 (1971). [https://doi.org/10.1016/0375-9474\(71\)90426-X](https://doi.org/10.1016/0375-9474(71)90426-X)
- [10] P.A. Moldauer, Phys. Rev. C, **14**, 764 (1976). <https://doi.org/10.1103/PhysRevC.14.764>
- [11] P.A. Moldauer, Nucl. Phys. A, **344**, 185 (1980). [https://doi.org/10.1016/0375-9474\(80\)90671-5](https://doi.org/10.1016/0375-9474(80)90671-5)
- [12] J. Kopecky, and M. Uhl, Phys. Rev. C, **41**, 1941 (1990). <https://doi.org/10.1103/PhysRevC.41.1941>
- [13] S. Goriely, and V. Plujko, Physical Review C, **99**(1), 014303 (2019). <https://doi.org/10.1103/PhysRevC.99.014303>

ЕМІСІЯ ВТОРИННИХ НУКЛОНІВ У ВЗАЄМОДІЇ ПРОТОНІВ З ЯДРАМИ  $^{12}\text{C}$ ,  $^{14}\text{N}$  AND  $^{16}\text{O}$

Рустам Муртазін<sup>1</sup>, Степан Карпусь<sup>2,1</sup>

<sup>1</sup> ННЦ «Харківський-фізико-технічний інститут» НАНУ, 1, Академічна, Харків, 61108, Україна

<sup>2</sup> Луцький Національний Технічний Університет, 75, Львівська, Луцьк, 43018, Україна

Представлено результати комп'ютерного моделювання виходу вторинних нейтронів та протонів при взаємодії протонів з енергією 50 MeV з легкими ядрами -  $^{12}\text{C}$ ,  $^{14}\text{N}$  та  $^{16}\text{O}$  за допомогою коду TALYS - 1.96 за замовчуванням. Важливість урахування випромінювання вторинних нуклонів - нейтронів та протонів є необхідним елементом при проведенні фундаментально-прикладних ядерних досліджень, таких як дозиметрія та радіаційна безпека. Як результат отримані повні перерізи утворення вторинних нейтронів та протонів, що вказують на суттєві відмінності в залежності від ядра-мішені. Для ядра  $^{12}\text{C}$  поріг утворення нейтронів знаходиться в області 20 MeV. Аналогічна характеристика для  $^{14}\text{N}$  лежить в області до 10 MeV, а для  $^{16}\text{O}$  поріг утворення нейтронів становить 17-18 MeV. Максимальний вихід нейтронів на один налітаючий протон спостерігається для ядра  $^{16}\text{O}$ . Також було визначено загальний переріз утворення вторинних протонів та їх вихід на один налітаючий протон. Як і у випадку з виходом нейтронів, ядро кисню демонструє найбільшу кількість вторинних протонів на протон, що дорівнює 1,47. Також були отримані розрахункові значення диференціальних перерізів від енергії вторинних протонів та нейтронів. Максимальне значення середньої енергії вторинних протонів спостерігається для ядра  $^{14}\text{N}$  і становить 12,72 MeV, тоді як для ядер  $^{12}\text{C}$  та  $^{16}\text{O}$  воно становить близько 10 MeV. Аналіз диференціальних перерізів від енергії вторинних нейтронів показав, що максимальне значення середньої енергії для нейтронів, отримано в результаті взаємодії з ядром азоту, тоді як енергії вторинних нейтронів, що утворюються на ядрах  $^{12}\text{C}$  та  $^{16}\text{O}$ , приблизно рівні (6,2 та 6,4 відповідно).

**Ключові слова:** легкі ядра; вторинні нуклони; TALYS